ACS APPLIED MATERIALS & INTERFACES

Research Article

www.acsami.org

Minimizing Isolate Catalyst Motion in Metal-Assisted Chemical Etching for Deep Trenching of Silicon Nanohole Array

Lingyu Kong,[†,‡,§] Yunshan Zhao,[§] Binayak Dasgupta,[†,‡] Yi Ren,[‡] Kedar Hippalgaonkar,[‡] Xiuling Li,[*,∥] Wai Kin Chim,[*,§] and Sing Yang Chiam[*,‡]

[†]NUS Graduate School for Integrative Sciences and Engineering, National University of Singapore, 28 Medical Drive, Singapore 117456

[‡]Institute of Materials Research and Engineering, A*STAR (Agency for Science, Technology and Research), 2 Fusionopolis Way, Innovis, Singapore 138634

[§]Department of Electrical and Computer Engineering, National University of Singapore, 4 Engineering Drive 3, Singapore 117583

[∥]Department of Electrical and Computer Engineering, Micro and Nanotechnology Laboratory, University of Illinois at Urbana−Champaign, Urbana, Illinois 61801, United States

Supporting Information

ABSTRACT: The instability of isolate catalysts during metal-assisted chemical etching is a major hindrance to achieve high aspect ratio structures in the vertical and directional etching of silicon (Si). In this work, we discussed and showed how isolate catalyst motion can be influenced and controlled by the semiconductor doping type and the oxidant concentration ratio. We propose that the triggering event in deviating isolate catalyst motion is brought about by unequal etch rates across the isolate catalyst. This triggering event is indirectly affected by the oxidant concentration ratio through the etching rates. While the triggering events are stochastic, the doping concentration of silicon offers a good control in minimizing isolate catalyst motion. The doping concentration affects the porosity at the etching front, and this directly affects the van der Waals (vdWs) forces between the metal catalyst and Si during etching. A reduction in the vdWs forces resulted in a lower bending torque that can prevent the straying of the isolate catalyst from its directional etching, in the event of unequal etch rates. The key understandings in isolate catalyst motion derived from this work allowed us to demonstrate the fabrication of large area and uniformly ordered sub-500 nm nanoholes array with an unprecedented high aspect ratio of ∼12.

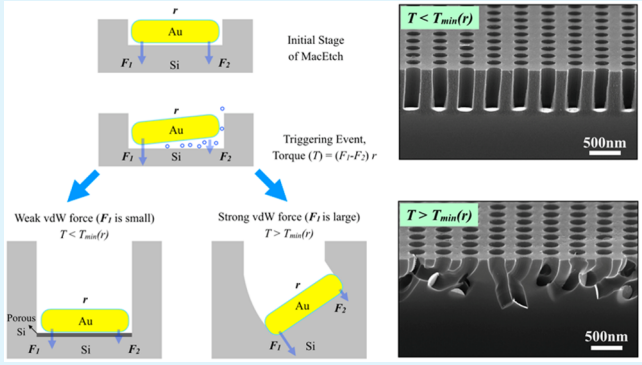

KEYWORDS: *metal-assisted chemical etching, silicon, isolate catalyst, van der Waals force, Raman analysis, porous silicon*

1. INTRODUCTION

Metal-assisted chemical etching (MacEtch) is a powerful technique for fabricating a large range of microstructures/nanostructures on both silicon (Si) and compound semiconductors.[1−6] The simplicity, versatility, and cost effectiveness of the approach provided the motivation to explore the use of the technique for applications in many different areas over the past two decades. These include electronics, optoelectronics, biological/chemical sensors, optical devices, and energy harvesting applications.[7−12]

Fabricating nanowires using MacEtch is now relatively routine, even for wires with high aspect ratios.[13,14] One key reason behind this success is the stability of the large mesh catalyst structure used for the etching of the wires. The bending torque required to deviate any catalyst from its downward etching direction is directly proportional to both the applied force and the radius from the pivoting point. The latter scales with the size of the mesh, and thus a larger mesh requires a larger minimum force for deviating the catalyst motion.[15] Hildreth et al. found from deformation calculation that such a force should be at least ∼0.5 MPa while Lai and Choi estimated a value of ∼2.5 MPa for larger gold (Au) mesh.[15,16] Isolate catalyst, especially of smaller dimensions, requires much less minimum bending torques, and thus catalyst motion during etching is a common and persistent problem.[9,17−23] This poses a significant road block to the potential applicability of MacEtch in high aspect ratio hole etching in the field of biological/water filters,[24] nanophotonics,[25] and the through-silicon-via etching.[26]

Unfortunately, this is not an easy problem to solve as isolate catalyst MacEtch is probably a dynamic process with changing parameters as etching proceeds. While there are numerous reports on isolate catalyst etching, isolate catalyst motion

Received: March 31, 2017
Accepted: May 23, 2017
Published: May 23, 2017

DOI: 10.1021/acsami.7b04565
ACS Appl. Mater. Interfaces 2017, 9, 20981−20990

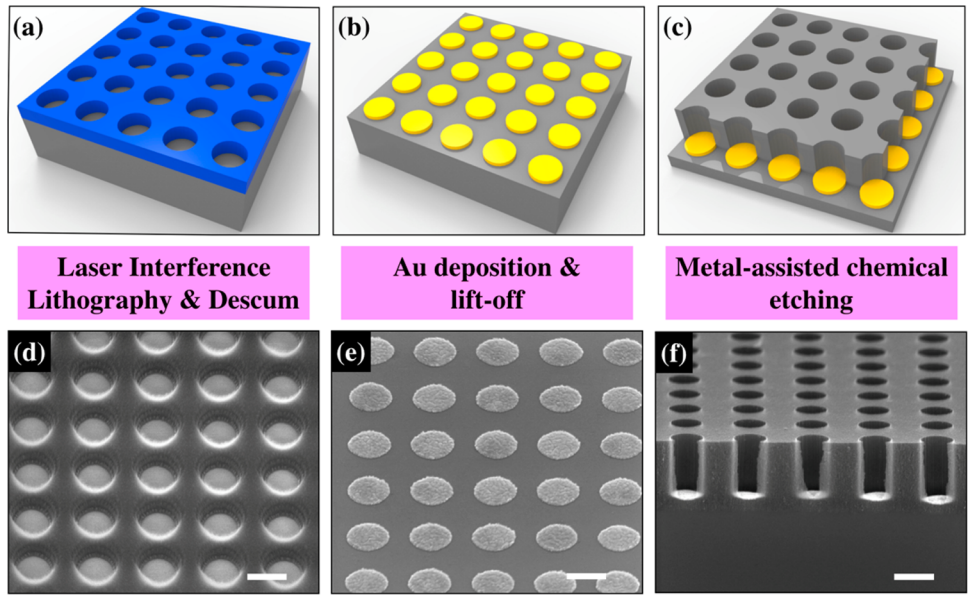

Figure 1. Schematic showing the main steps of process flow in the fabrication of silicon (Si) nanoholes array by laser interference lithography. (a) Laser interference lithography and oxygen descum. (b) Gold (Au) evaporation and lift-off. (c) Metal-assisted chemical etching to form Si nanoholes array. The corresponding SEM micrographs of each step are shown in (d, e) at 45°-tilt view and (f) at 75°-tilt view. Scale bars are 500 nm.

remains fundamentally not well understood.[9,15,17−22,27−32] There have been a few reported works that address the origin of the catalyst motion and factors influencing it. Peng et al. have suggested that electrophoresis can be the driving phenomena in causing catalyst motion. The generated field from differences in the charge transport during the MacEtch process causes the deviation of the catalyst from its vertical downward etching direction.[27] However, Hildreth et al. have recently estimated electrophoretic forces from etch rates considerations and found them to be too small to account for the required torques in moving the catalyst. Instead, they discussed how van der Waals (vdWs) forces can produce the necessary pressure for such deviations.[15,31] If vdWs adhesion forces between the catalyst and semiconductor are sufficient to produce the deviating catalyst motion, it is critical to understand the primary causes that trigger the deviation or factors that can affect the strength of the vdWs attraction. From the survey of the reported works, we hypothesize that unbalanced etch rates across a catalyst can be a triggering event. Any differences in etch rates coupled with high vdWs forces can pull a catalyst toward the direction with a relative lower etch rate, thereby deviating the catalyst from the downward vertical motion. Lee and co-workers reported on the importance of catalyst symmetry and demonstrated the etching of deep and vertical pores using spherical metal particles.[29] The unbalanced etching can possibly be prevented by the use of isotropic spherical particles, so that the etch rate variations caused by catalyst thickness variation or transport processes are reduced.[29] The importance of geometry in affecting catalyst motion is also shown by Hildreth and co-workers when they found that small or asymmetric catalysts are generally most prone to movement during etching.[16,18,23,31] Asymmetric catalysts can cause differences in etch rates due to the differences in shapes or exposed edges that can better facilitate the transport of etchant/reactant. The explanation using unbalanced etch rates can also be compared against the model proposed by Sakdinawat and Chang.[19,20] The latter reported on the nonuniform distribution of electrons and holes (etch rates) in the deviation of the isolate catalyst, which is reduced when larger catalyst strips are placed near the isolate catalysts to reduce the carriers splaying effect.[19,20] Finally, we believe that the unbalanced etch rate explanation is also consistent with the suggestion that the perturbation from hydrogen gas produced during etching is the cause for catalyst motion.[22] In this case, the hydrogen gas produced at the interface can change the etch through a hindering of transport/transfer processes and hence trigger the deviating motion of the catalyst.

Some of the triggering causes of the catalyst deviation, as discussed, are very difficult to prevent. Even when we restrict the etching to only isotropic catalyst geometries, catalyst thickness and regularity are still susceptible to variations while hydrogen gas evolution is dynamic and difficult to eliminate. For example, in the etching of holes array patterned using optical lithography and catalyst metal evaporation, slight differences in the catalyst thickness due to shadowing effects are common. Irregularity, in terms of interspacing or the size of the eventual isolate catalyst, is even more pronounced when self-assembly type of fabrication is used. It is thus not surprising that reports in the etching of such isolate catalyst always produced unwanted motion during the process.[17,22,27,28] Recently, attempts to etch with large area and regular ordered Au catalyst array, even with surrounding large Au structures for carriers balancing, resulted in mixed success with observation of both vertical and nonvertical etching behaviors.[9,12,19−21,32,34,35] The most successful result was shown by Brodeceanu et al.,[32] where the isolate catalyst motion is minimized, and the authors have attributed this to the use of extremely uniform and isotropic Au catalyst.[32] Since it might be challenging to totally eliminate most of the triggering mechanisms, the ability to minimize isolate catalyst motion may lie in the knowledge and ability to tune the vdWs force at the interfaces. Therefore, in this work, we attempt to vary the interface forces through the creation of porous Si via different etchant concentration or doping concentration. We employ regular arrays of isolated Au discs for the etching of regular holes to try to keep the geometry, spacing, and thickness of the catalyst constant. We

DOI: 10.1021/acsami.7b04565
ACS Appl. Mater. Interfaces 2017, 9, 20981−20990

provided clear experimental evidence to show how a higher hydrofluoric acid:hydrogen peroxide ($HF:H_2O_2$) ratio or a higher p-type Si doping can lead to reduced isolate catalyst motion. We provided evidence that the higher doping drastically reduces catalyst motion through the creation of porous Si, and this can be interpreted through a reduction of the vdWs forces at the interface. Our results from the different oxidant ratio also show that utilization of such a phenomenon has to be balanced with a suitable etching rate. We attribute this to the generation of more triggering mechanisms from either hydrogen generation or mass transport variations that can eventually result in the unwanted catalyst motion. Using our findings, we demonstrated the successful fabrication of large area, regular ordered, and vertical Si nanoholes array with a high aspect ratio of ~12 for the first time.

2. EXPERIMENTAL SECTION

Si (100) substrates of three different boron doping concentration, 4−8 Ω·cm (p^-), 0.1 Ω·cm (p), and 0.005 Ω·cm (p^+), were used for the MacEtch experiments. The samples were precleaned by sonication in acetone, followed by isopropyl alcohol (IPA) for durations of 15 min each. They were subsequently rinsed in deionized (DI) water and blown dry by a nitrogen gun. A further native oxide removal step is not performed since the following catalytic etching will not be affected.[2] An illustration of the fabrication steps and corresponding scanning electron microscope (SEM) images are shown in Figure 1. Negative photoresist (ma-N1407) of 500 nm thickness was spin-coated onto the samples. The pre-exposure bake at 95 °C for 60 s was carried out, before patterning using laser interference lithography via a He−Cd laser (wavelength of 325 nm) with a Lloyd's mirror setup.[36] The photoresist array pattern was generated using two exposures at right angles to each other, yielding nanoholes array with a typical depth of ~400 nm, diameter of ~450 nm, and spacing of ~400 nm. The pattern was subsequently descummed by oxygen plasma in a Sirus Trion reactive ion etching (RIE) system for 10−20 s. The descummed step ensures the removal of any residual resist that might restrict the etching or cause any isolate catalyst motion. Gold catalyst of 23 ± 3 nm was evaporated onto the patterned samples using an Edwards Auto 306 FL400 thermal evaporator. The evaporation pressure was typically $\sim 2 \times 10^{-6}$ mbar, and the evaporation rate was controlled to be 1.5 Å/s as monitored in situ by a quartz crystal microbalance. The photoresist and excess metal were removed by sonication in acetone for 5 min, leaving behind a periodic Au discs array. The catalytic etching was conducted at room temperature in a yellow light environment. The MacEtch solution consists of 13.5 M HF with varying molar concentration of H_2O_2 (0.16, 0.48, 0.91, and 1.43 M) and DI water. MacEtch was performed for durations of 5−65 min, depending on the experimental requirements. After etching was completed, the etched samples were rinsed in DI water before drying on hot plate at 50 °C for 1−2 min. The fabricated Si nanoholes array cross sections were imaged using the Nova NanoSEM 230. To quantitatively study the porosity of etched nanoholes structure for p-type Si with different doping concentration, Raman analysis was carried out using Raman spectroscopy (WITec Alpha 300) with a 532 nm (2.33 eV) laser excitation source, and a laser spot size of ~1 μm was used. The Voigt function (convolution of a Lorentzian with a Gaussian line shape) is fitted to each of the Raman peaks in order to determine the peak frequency and full width at half-maximum (fwhm).[37] To characterize the size and distribution of pores within the MacEtch sample at the atomic level, high-resolution (HR) transmission electron microscopy (TEM) using the JEOL JEM 2100 was carried out. The TEM sample preparation was performed by sonication of the MacEtch Si nanowires (same etching condition as MacEtch of nanoholes) in ethanol for 1 min immediately after etching. The suspended Si nanowires in ethanol were then transferred to a carbon−copper grid for the TEM analysis.

3. RESULTS AND DISCUSSION

3.1. Effect of Oxidant and Silicon Doping Concentration on Isolate Catalyst Motion. Formation of porous Si is a well-known phenomenon which has been observed in MacEtch. Depending on etching conditions, pores with different density and thickness can be found at the catalyst/Si interface, along the sidewalls, and within the etched Si nanostructures.[7,13,38−45] In general, the concentration of the porosity is positively correlated to oxidant and silicon doping concentrations, whereby a higher oxidant concentration or higher Si doping concentration results in higher levels of porosity.[7,13,38−45] In this work, we systematically varied the oxidant concentration of MacEtch across three different doping concentration of p-type Si (p-Si). Unlike other studies, we calibrated the etching rate for the different conditions and deliberately attempted to vary the etching duration to maintain a similar etching depth of ~1.8 ± 0.3 μm. This is important to ensure a fair comparison across the different conditions by keeping the amount of Si removal and the etching depth similar. The motion of the catalyst is examined by SEM cross-section images (75°-tilt view) of the resultant nanoholes as shown for the p-Si in Figure 2. The images for the MacEtch p^--

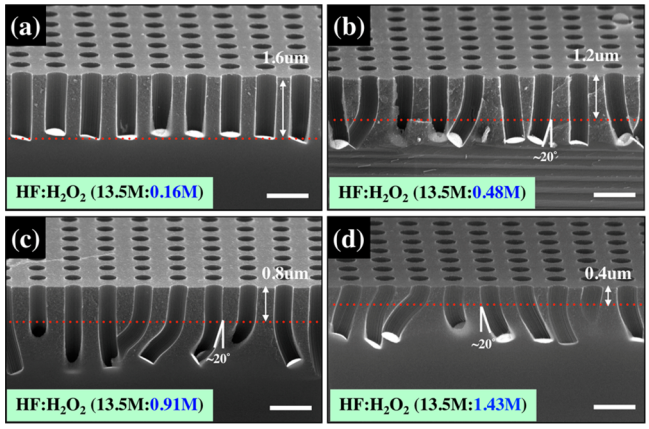

Figure 2. Cross-section SEM micrographs (75°-tilt view) of MacEtch Si nanoholes array on p-Si (0.1 Ω·cm) substrate in etching solution of constant HF concentration (13.5 M) and varying molar concentrations of H_2O_2 of (a) 0.16, (b) 0.48, (c) 0.91, and (d) 1.43 M. The depth of holes is maintained relatively the same at ~1.8 ± 0.3 μm for the four different solutions. The critical depth is shown as a dotted red line in the micrographs, where most (>50%) of the catalysts deviate by more than the indicated 20° from the downward vertical motion. The etching trajectory is straight at low H_2O_2 concentration but becomes unstable and eventually random as the H_2O_2 concentration is increased. Scale bars are 1 μm.

and p^+-Si samples are shown in Figures S1 and S2 (Supporting Information). While the overall stability of the catalyst motion can be immediately apparent, we introduce a more quantitative examination by defining an average critical depth (∂, nm). ∂ is taken to be the depth where most (>50%) of the catalysts deviate by more than 20° (as indicated in the SEM images) from its downward vertical motion. The representative ∂ is also shown as a dotted red line in the micrographs. Figure 2a−d shows the effect of varying the H_2O_2 oxidant concentration from 0.16 to 1.43 M, with a constant HF concentration. It can be observed that the lowest oxidant concentration of 0.16 M shows almost no isolate catalyst motion, while such instability increases with increasing oxidant concentration. The lowest

DOI: 10.1021/acsami.7b04565
ACS Appl. Mater. Interfaces 2017, 9, 20981−20990

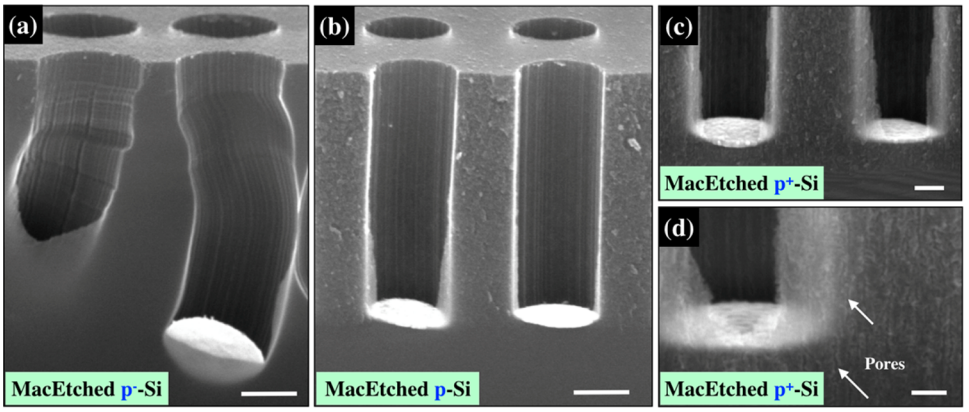

Figure 3. High-resolution cross-section SEM micrographs (75°-tilt view) of MacEtch Si nanoholes array on (a) p^--Si, (b) p-Si, (c) p^+-Si in 13.5 M HF and 0.16 M H_2O_2 and (d) p^+-Si in 13.5 M HF and 0.91 M H_2O_2. No porous Si can be clearly observed either at the nanoholes sidewall or Au discs/Si interface for the MacEtch p^--Si, but such porosity is observed for p-Si and p^+-Si at both the sidewall and Au/Si interface. Scale bars are 300 nm for (a–c) and 100 nm for (d).

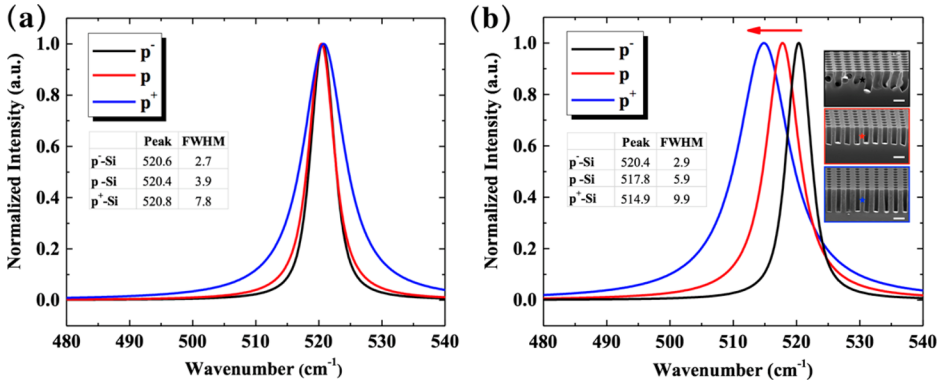

Figure 4. Raman spectrum of (a) unetched p^-, p, and p^+ crystalline Si samples and (b) MacEtch p^-, p, and p^+-Si nanoholes array samples. The etching solution consists of 13.5 M HF and 0.16 M H_2O_2. The stars in the inset of the SEM images (scale bar of 1 μm) indicate the Raman laser probe locations. The normalized peak positions and fwhm of Si and Si nanoholes samples with different doping concentrations are summarized in the inserted table for both the etched and unetched samples.

oxidant concentration of 0.16 M yields a ∂ value of ~1.6 μm while the critical depth reduced drastically to ~0.4 μm for the highest oxidant concentration of 1.43 M. This trend of decreasing critical depth with increasing oxidant concentration is observed across all three different Si doping concentration. However, ∂ is generally higher for a higher Si doping concentration. Figure S1 shows that for p^--Si ∂ varies from ~800 nm to well below 200 nm, whereby some catalyst deviating motion can even be observed at the very onset for the higher oxidant concentration. On the contrary, Figure S2 shows that for p^+-Si the catalysts remain relatively stable except when the highest oxidant concentration of 1.43 M is used. The trends in the variation of the Si doping and oxidant concentration will be discussed in greater detail in the final section.

3.2. Examining the Porosity of Etched Structures. The clear correlation of reduced catalyst motion with a lower oxidant ratio, and especially with a higher substrate doping, suggests that the porosity of Si during etching might play a major role in affecting the catalyst motion. The high resolution SEM images of MacEtch p^--, p-, and p^+-Si are shown in Figure 3. For the catalyst with deviating motion, as observed for the p^--Si in Figure 3a, both the etched sidewalls and catalyst–Si interface appeared to be smooth. Comparatively, for the p-Si (Figure 3b) and p^+-Si (Figure 3c,d) samples that yielded little or no catalyst motion, rough structures that correspond to porosities are observed on the etched sidewalls and at the catalyst–Si interface. The observation of porosity during etching for similar etching conditions is consistent with reports of MacEtch Si wires from other works.[13,41] We add that the extent of porosity appears to be greatest for the p^+-Si. This can be seen from the extended roughened area, especially near the catalyst–Si interface as shown in Figure 3d.

Comparing the extent of porosity among the etched Si structures is difficult if it is accomplished solely with microscopy-based techniques.[13,38,44] These techniques are important to show the average size and existence of pores but fall short in giving a more quantitative representation of the porosity concentration. Raman scattering spectroscopy is an effective tool to study the optical and acoustic phonons in Si that can be fundamentally linked to scattering sites, such as defects, porosity, or surface roughness.[46−48] Examination of phonon scattering characteristics using Raman spectroscopy has been successfully employed to study structures or the morphology of MacEtch nanowires.[46−48] Therefore, in this work, we will use Raman scattering measurements to provide a more quantitative comparison of the resultant porosity after MacEtch. The Raman spectra of unetched p-type Si substrates with different doping concentration are shown in Figure 4a, while the Raman spectra of corresponding MacEtch substrates using an oxidant concentration of 0.16 M are shown in Figure

DOI: 10.1021/acsami.7b04565
ACS Appl. Mater. Interfaces 2017, 9, 20981−20990

4b. The Raman peaks of the unetched Si substrates for all three doping concentration are located at around ~520.4 cm^{-1}, from the first-order Raman scattering of the longitudinal optical and transverse optical phonon modes of Si at the Brillouin zone center in crystalline Si, which is consistent with Raman spectra reported in other works.[46−48] The slight asymmetry and broadening of one-phonon Raman peak for the highly doped Si can be attributed to Fano interference, involving electron−phonon interactions of band-like states with discrete phonon states.[49,50] This is supported by the larger broadening on the higher wavenumber side that is characteristic of Fano type interaction. The Raman spectra for the MacEtch nanoholes are shown in Figure 4b. Unlike the measurement for the unetched Si substrate, whereby the laser probe (spot size of ~1 μm) was directed from the top of Si, the measurement for the etched holes directed the laser probe at the cross section of the MacEtch structures, as depicted by the star symbol in the inset of Figure 4b. This was done to eliminate contribution from the unetched Si substrate. The Raman peak of the etched p^--Si is at 520.4 cm^{-1}, which indicates zero or minimal red-shift. This is different from the clear red-shift of 2.6 and 5.5 cm^{-1} that is observed for p-Si and p^+-Si, respectively, with the concomitant broadening of the fwhm. A red-shift and asymmetric broadening of the first-order phonon mode in the Raman spectra can broadly be attributed to three origins, namely phonon confinement effect, compressive strain effect, and inhomogeneous heating effect.[51] The phonon confinement effect should only show up for Si nanostructures with dimensions of 20 nm or less.[52,53] The compressive strain effect that results from native oxide stresses is typically small.[51] Therefore, we attribute the Raman peak shift observed in this work to localized inhomogeneous heating. The shift is caused by poor heat dissipation that can be directly related to the porosity of the Si investigated.[46,53] The etched Si structures with porosity cannot adequately dissipate the localized laser heating and the thermally excited lattice phonons, and this causes a red-shift and broadening of the Raman peaks from anharmonic scattering effects.[46] The Raman spectra for the other etchant concentration (i.e., higher oxidant concentration ratio) are shown in Figure S3. A similar conclusion can be drawn whereby the porosity of the etched structures is significantly affected by the doping level of the substrate. Interestingly, comparing the Raman peak shifts for the same doping concentration across different etchant concentration shows a smaller variation in the porosity. This may be due to the boundary we have set in formulating the experiments: while a higher oxidant concentration ratio is expected to increase the porosity of the etched Si, this may be brought about by the different etching rates if the same etching duration is employed. For example, in trying to maintain similar etch depths or lengths, a higher oxidant concentration is balanced by a shorter etching duration in our work. The similar porosity observed across the different oxidant concentration suggests that the etch depth may instead serve as a good normalization guide to the level of porosity generated. Moreover, the HF:H_2O_2 ratio used in this work is significantly higher. This can suppress the formation of porosity even with a higher oxidant concentration since the removal of the carriers by etching is now not a limiting factor. It is also worth noting that the porosity created exhibits an axial gradient.[47] We verified this with a Raman spectroscopy line scan (Figure S4) that shows increasing porosity from the base of the Si nanostructure to the tip. Such a porosity grading methodology and understanding will be of interest to communities that are interested in controlling and utilizing Si nanostructures with graded porosity.

The porosity of the etched samples is further examined using HRTEM to verify the crystallinity. Instead of examining the sidewalls of the etched holes, we study p^+-Si nanowires etched using the same etching conditions (13.5 M HF:0.91 M H_2O_2), as shown in Figure 5a. In this approach, not only can we examine the porosity of a single wire, which is representative of the sidewalls of the etched holes, we also avoided issues with isolate catalyst motion with the use of larger size meshes. Figure 5b shows the TEM micrograph of a p^+-Si nanowire, and the diffraction pattern in the inset indicates that the core structure remains crystalline. Mesoporosity along the wire walls, with pore sizes of <10 nm, can be observed from the HRTEM image in Figure 5c, which is in good agreement with other reported works.[13,44] Importantly, the HRTEM image shown in Figure 5d shows clearly the presences of the pores and together with clear lattice fringes showing that the crystalline structure has been preserved. The image also shows possible slight oxidation observed along the walls of the pores.

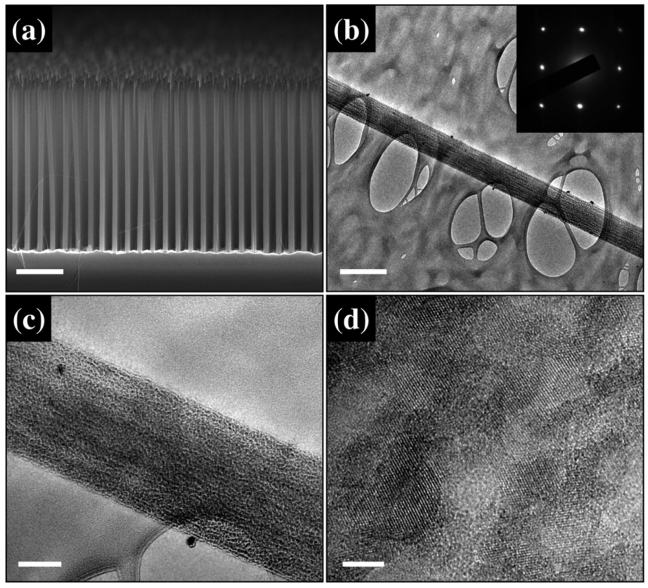

Figure 5. Structural characterization of MacEtch porous p^+-Si nanowires etched using identical etching solution (13.5 M:0.91 M of HF:H_2O_2) employed for the MacEtch of the nanoholes array. (a) A cross-section SEM image of the etched porous nanowire array. The nanowires are vertically oriented on the p^+-Si substrate. (b) TEM micrograph of the porous nanowire. The inset diffraction pattern indicates that the nanowire is single crystalline. (c) HRTEM image of the surface of the porous Si nanowire showing the network of nanocrystalline Si. (d) HRTEM images of the Si near the interior pores region of the nanowire. The pore size can be estimated to be <10 nm. The crystal lattice can be observed continuously around the pores. Scale bars are 3 μm for (a), 500 nm for (b), 100 nm for (c), and 5 nm for (d).

3.3. Role of Porosity: vdWs Forces and Etch Rates. As we have discussed in the previous section, the porosity of the etched Si is affected primarily by its doping concentration and to a lesser extent by the H_2O_2 concentration. This is more clearly shown in a summary plot of the porosity level (represented by the Raman peak position or its shift) and the H_2O_2 concentration in Figure 6a. The porosity levels do not vary greatly across the different H_2O_2 concentration, unlike the

DOI: 10.1021/acsami.7b04565
ACS Appl. Mater. Interfaces 2017, 9, 20981−20990

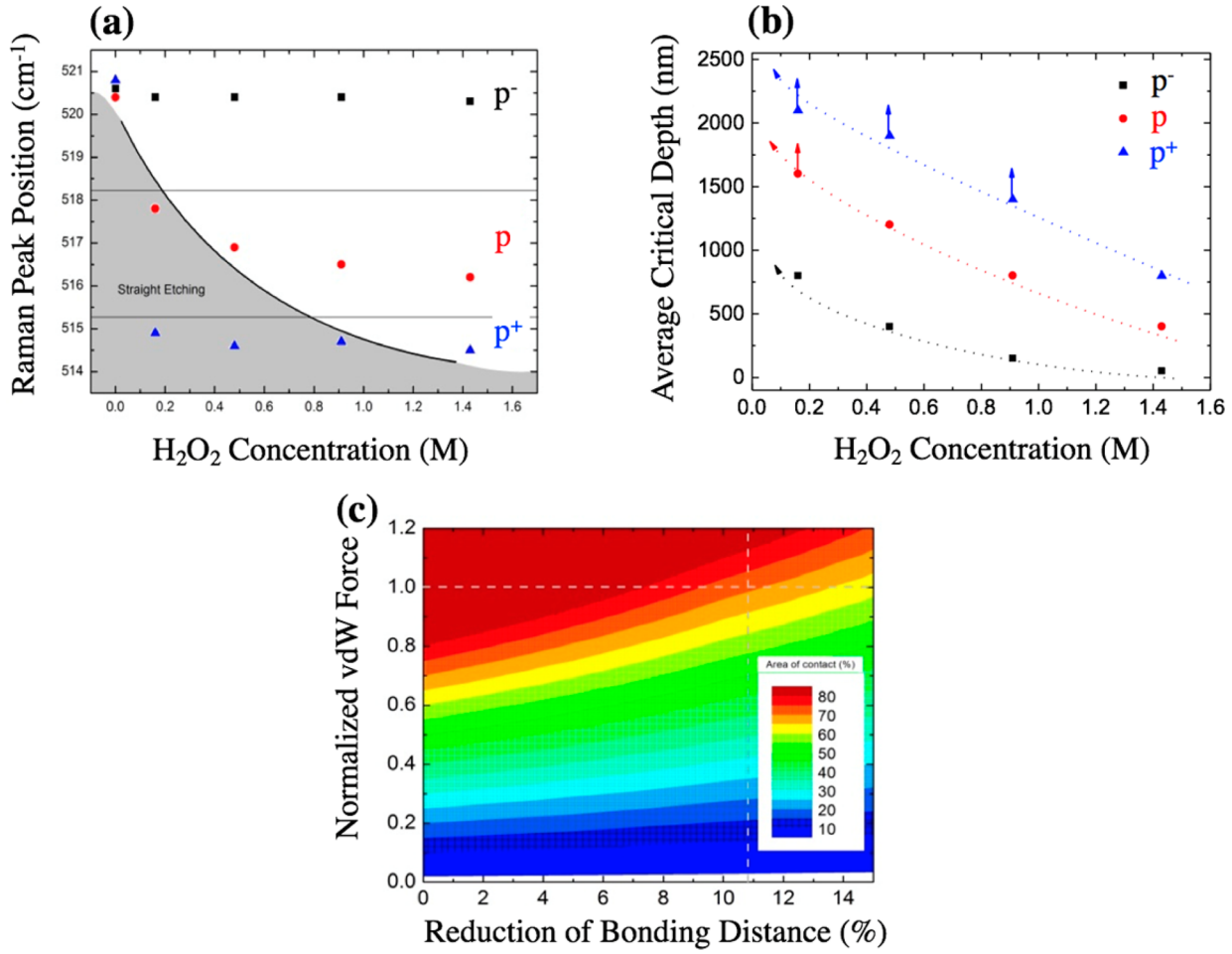

Figure 6. Analysis of the role of porosity on isolate catalyst motion. (a) Raman peak position (porosity of etched Si sample) as a function of Si doping concentration and H_2O_2 concentration. (b) Effect of H_2O_2 concentration on the achieved average critical depth for the three different Si doping concentrations. When the data point indicates a lower bound value of the critical depth, they are marked with arrows. The dotted lines are indicated as a visual guide. (c) Contour plot showing the normalized vdWs forces variation with bonding distance and area of contact between Au and Si.

variation with the Si doping concentration. The shaded gray area indicated in Figure 6a represents conditions whereby reduced catalyst motion is achieved for our targeted etch depth of ~1.8 ± 0.3 μm. The achieved average critical depth for the various conditions is shown in Figure 6b. It is once again clear that the doping concentration, and hence porosity, has a significant impact in deciding the average critical depth. However, the trend presented also shows clearly that the H_2O_2 concentration has a role to play in deciding isolate catalyst motion; from the similar Raman peak positions measured and shown in Figure 6a, this cannot be directly linked to the porosity. While a similar etch depth is targeted, the different H_2O_2 concenetration still corresponded to different etch rates. This can be more clearly shown by plotting the achievable critical depth for the varying etch rates we investigated, as shown in Figure S5a. The average etch rate for different oxidant concentrations represents averaged measurements from sets of 15 nanoholes for more than four samples of each condition, as shown in Figure S5b. A lower etch rate (lower H_2O_2 concentration) promotes better stability of the isolate catalyst as shown by the larger recorded critical depths for all doping concentration. We believe that a faster etch rate can exacerbate any unequal etching that is a triggering event for isolate catalyst motion. Therefore, in short, the etch rate affected the triggering events of unequal etching, while the porosity affected the likelihood of isolate catalyst deviation upon such events.

We can further elaborate on how porosity affected the likelihood of isolate catalyst motion. The presence of porosity can lead to better stabilization through the reduction of the vdW forces that decreases the bending torque forces. In the event that there are unequal etch rates across the catalyst, chances of catalyst motion are reduced when the bending torques are smaller. The general vdWs attraction force between two flat surfaces can be represented as[54]

$$F_{\mathrm{vdW}} = \frac{C}{6\pi d^3} A \tag{1}$$

where C is the Hamaker constant, d is the separation between the catalyst and the Si substrate, and A is the total contact area between gold film and Si substrate. The porosity can affect the vdWs forces by either altering the separation between the Au and Si or reducing the effective contact area between the two surfaces. Since these are opposing contributions to the eventual vdW force, we plotted a normalized vdWs force contour plot in Figure 6c to showcase scenarios of reducing area and bonding distance. The normalization is against the vdW force value before the generation of pores, so any value below 1 represents

DOI: 10.1021/acsami.7b04565
ACS Appl. Mater. Interfaces 2017, 9, 20981−20990

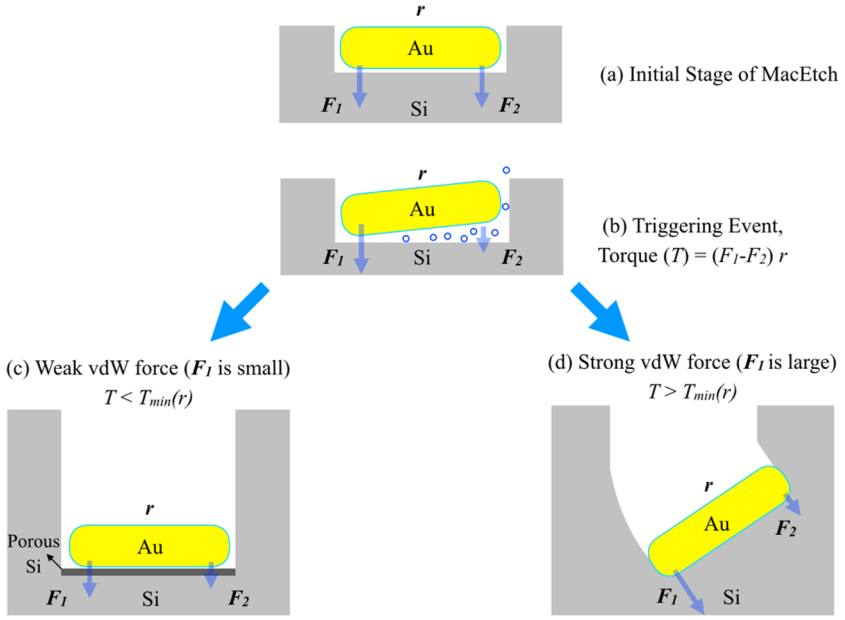

Figure 7. Schematic showing the effect of vdWs force on the motion of the isolate catalyst during Si MacEtch. (a) The Au catalyst is in intimate contact with the Si substrate by vdWs attraction force at the initial stage of MacEtch. (b) Triggering event brought about by unequal etch rates or bubbles generation. (c) If the bending torque is smaller than $T_{min}(r)$, in the case of weak vdWs forces, the catalyst motion proceeds in the vertical direction. (d) If the bending torque is larger than $T_{min}(r)$, in the case of strong vdW forces, the catalyst tends to deviate from its downward vertical direction.

a reduction in the vdW force. It is likely that the creation of porosity does not lead to any significant changes in bonding distance as the catalyst must still interact with the topmost Si surface. Nonetheless, an estimation for the bonding distance variation can be made using the Lennard-Jones potential, and this amounts to a maximum reduction of ∼10.9% in the bonding distance (Supporting Information S6).[55] This value is shown as a vertical dotted line in Figure 6c, indicating that an ∼70% contact area will definitely yield a reduction in vdWs force, irrespective of the bonding distance. The reduction in vdWs force (areas under the horizontal dotted line) directly translates to smaller bending torques and thus higher probability of vertical etching motion in the event of unequal etch rates. Interestingly, if we examine the p^+-Si, whereby most of the samples produce the vertical etching, the percentage porosity as measured from an electron beam heating technique is ∼35% (Supporting Information S7). This is in good agreement with the estimated value from the plot in Figure 6c if we assume an isotropic distribution of the porosity. From the same plot, it can also be said that any introduction of porosity of less than 20% will only reduce the vdWs force if the bonding distance change is less than 7%. Otherwise, it will not aid in stabilizing isolate catalyst motion via vdWs force changes.

While the doping concentration can clearly affect the porosity and hence the vdWs force as discussed, the effect of a higher H_2O_2 concentration is not as straightforward. Thus, the effects of HF:H_2O_2 molar ratio on the motion of isolate catalyst during MacEtch appears to be controversial with differing experiment results. Hildreth et al. found that using etchants with low HF:H_2O_2 molar ratio (HF/(HF + H_2O_2) of 40%) helps to stabilize the motion of catalysts during MacEtch that results in more uniform etching.[18] However, the geometry of most catalysts studied in the aforementioned work is irregular or asymmetric (anisotropic), and it might be difficult to draw a clear conclusion about the oxidant concentration without decoupling the catalyst geometry effect. On the contrary, fabrication of high aspect ratio Si nanostructures with high HF:H_2O_2 molar ratio (HF/(HF + H_2O_2) of 96% has been shown to be possible, but again, that is achieved only with balancing and anchoring patterns.[19] For regular ordered Au or Ag discs array pattern, MacEtch using a high HF:H_2O_2 ratio is normally employed, and the etching results are not consistent.[9,12,21,32,34] In our work that better represents a control experiment, the patterns are balanced, isotropic, and consistent. We have also tried to ensure that the higher oxidant concentration translates only to a higher etch rate with different etching duration to keep the etch depth constant. Thus, the resultant average critical depth variation as a result of the different oxidant concentration (Figure S5a) can be interpreted solely as an etch rate phenomenon. We believe that a larger etch rate represents a higher rate of etchants and byproducts transport. In addition, there will be a higher rate of hydrogen gas generation at the interfaces during etching.[1,22] Such increased rate of mass transport and bubbles generation is a source of turbulence at the etch front that can trigger the unequal etch rates in a localized region. The unequal etch rate distribution along the catalyst creates bending torques across the catalyst, as dictated by the vdW forces, and thus when these are sufficiently large, the isolate catalyst will deviate from its vertical etching direction.

The key findings in this work with regards to the isolate catalyst motion can be summarized in the schematic shown in Figure 7. During the MacEtch of an isolate catalyst, the catalyst remains in proximity to the Si substrate via the vdWs forces across the catalyst. In the schematic shown in Figure 7a, we simply represent this by only two forces, F_1 and F_2, across a generic length r. Vertical etching proceeds when the forces are not too different, especially across the catalyst dimension. During the process of etching, a triggering event that produces unequal etch rates might occur. These events can change the

DOI: 10.1021/acsami.7b04565
ACS Appl. Mater. Interfaces 2017, 9, 20981−20990

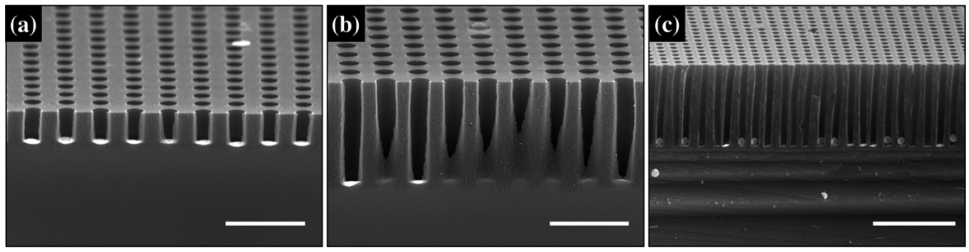

Figure 8. SEM micrographs (75°-tilt view) of Si nanoholes array showing the depth variation as a function of etching duration on p^+-Si in 13.5 M HF and 0.16 M H_2O_2: (a) 0.8 μm for 10 min, (b) 2.7 μm for 32 min, and (c) 5.4 μm for 65 min (aspect ratio is ∼12). Scales bar are 2 μm for (a) and (b) and 5 μm for (c).

effective forces on the catalyst and produce a resultant torque on the catalyst. Such triggering events are made more frequent in the case of higher etch rates as brought about by higher oxidant concentration. The effect of deviation with higher etch rates can also be further evidenced by etching at elevated temperature (Figure S8). Other possible triggering events or influencing factors can include bubbling, mechanical vibrations, gravitational forces, magnetic forces, and convective mass transport. In the most extreme example, where bubbling is the triggering mechanism, the vdWs forces and hence F_2 are significantly reduced, as shown in Figure 7b. The resultant torque acting on the catalyst will create a deviation if it surpasses the minimum torque, labeled as $T_{min}(r)$, required for rotation. This value is dependent on the size of the catalyst, whereby a larger $T_{min}(r)$ is required for larger catalyst size, thus explaining the stability of larger meshes. The resultant torque is greatly affected by the extent of the vdWs forces. In the case of the highly doped samples with high porosity, the vdWs forces are weak. Figure 7c shows that even with the triggering events, the torque produced is not sufficient for rotation ($T < T_{min}(r)$), and eventually the catalyst stills retains the vertical etching direction. When such porosity is absent and the vdWs force is sufficiently large ($T > T_{min}(r)$), the catalyst rotates and deviates from its etching position and proceeds with its trajectory until the next triggering event, as illustrated in Figure 7d.

While we have discussed about the effects of porosity (vdWs forces) and etch rate (mass transport and bubbling) separately, they need not be entirely independent. Geyer et al. have reported that the formation of a porous layer beneath the metal catalyst during MacEtch can facilitate the mass transport of the etchants and byproducts.[43,56] This means that the formation of porous Si can also help create an extra mass transport pathway, especially for high etch rate conditions, and this allows for a reduction in triggering events. Recently, Lai et al. have also suggested that a higher oxidant concentration (higher etch rate) can affect the vdWs forces by changing the bonding distance.[28] However, based on our experimental results, it appears that this effect can be small and the higher rate of triggering events dominates the stability of the isolate catalyst.

The new understanding we have proposed allowed us to achieve unprecedented deep trenching of Si nanoholes array. We fabricated deep trenches of nanoholes array by using p^+-Si with fine-tuned etching conditions. A longer duration MacEtch using 13.5 M HF and 0.16 M H_2O_2 (slow etching rate) showed excellent results, whereby large area nanoholes array with excellent uniformity and high aspect ratio is achieved (Figure S9). Figure 8 shows the ability to control the fabricated Si nanoholes by simply varying the etching duration, where ordered arrays of vertically aligned nanoholes is demonstrated. The achieved depth of ∼5.4 μm (Figure 8c) for the ordered nanoholes array is to our knowledge the highest achieved aspect ratio (∼12) for sub-500 nm nanoholes. The closest work was shown by Brodoceanu and co-workers where they achieve an aspect ratio of ∼5.3 for vertical nanoholes of ∼850 nm in diameter.[32] It is also notable that our achieved nanoholes array was fabricated without the assistance from any external influences such as anchoring structures, electron−hole balance structures, or magnetic forces.[9,19,20] The ability to etch such vertical pore arrays can prove to be important for a variety of applications. The periodic arrays of nanoholes shown in this work can allow the use of the simple and low-cost MacEtch technique in areas such as sensors, solar cells, photonic crystals, functional semiconductor metamaterials, creation of through-Si via (TSV), and filtration.[24−26,57] This can possibly replace the current commonly employed methods such as plasma-assisted dry etching or electrochemical etching process.

4. CONCLUSIONS

We have developed in this work a greater understanding of isolate catalyst etching. We show that the doping concentration of Si significantly affects the generation of porous Si during etching. The porosity, in turn, critically affects the stability of the isolate catalyst motion. We showed that enhanced stability can be attributed to a reduction of the vdWs forces through a reduction in the contact area of the catalyst and the semiconductor. Lower vdWs forces produce a lower bending torque that is responsible for deviating the downward etching of the isolate catalyst. Using this understanding, we predicted that a porosity level greater than 20% can be sufficient in lowering the vdWs force while any porosity greater than 30% will most certainly lead to enhanced catalyst stability. We also show that the control of the oxidant concentration affected the etch rate of the process, and under control conditions, a lower etch rate leads to more stable isolate catalyst etching. We attribute the instability to a larger occurrence of unequal etch rates that we predict are triggering events to start the isolate catalyst deviation. The unequal etch rates occurrences are elevated by larger mass transport and/or bubbles formation under a higher etch rate condition. Finally, the stability of the isolated catalyst array is shown in this work via the fabrication of large area, uniform, and regular ordered sub-500 nm nanoholes array with an unprecedented high aspect ratio (∼12).

■ ASSOCIATED CONTENT

Supporting Information

The Supporting Information is available free of charge on the ACS Publications website at DOI: 10.1021/acsami.7b04565.

DOI: 10.1021/acsami.7b04565
ACS Appl. Mater. Interfaces 2017, 9, 20981−20990

MacEtch results of p^--Si as a function of H_2O_2 concentration; MacEtch results of p^+-Si as a function of H_2O_2 concentration; Raman spectrum of MacEtch p^--, p-, and p^+-Si nanoholes samples with different H_2O_2 concentration; Raman spectroscopy line scan of MacEtch p^+-Si nanoholes sample; relation among critical depth, average etch rate, and H_2O_2 concentration; estimation for bonding distance variation between Au catalyst and Si using the Lennard-Jones potential model; porosity of porous Si nanowire characterization; MacEtch results of p^+-Si at elevated tempature; uniformity of MacEtch Si nanoholes array (PDF)

AUTHOR INFORMATION

Corresponding Authors

*E-mail: chiamsy@imre.a-star.edu.sg (S.Y.C.).
*E-mail: elecwk@nus.edu.sg (W.K.C.).
*E-mail: xiuling@illinois.edu (X.L.).

ORCID

Sing Yang Chiam: 0000-0002-5157-3533

Author Contributions

L.Y.K. designed and performed all experiments. Y.Z. assisted with the Raman spectroscopy and TEM characterization. L.Y.K., X.L., S.Y.C., and W.K.C. performed data analysis and wrote the manuscript. S.Y.C. and W.K.C. supervised the project. All the authors discussed the data and commented on the manuscript. All authors reviewed the manuscript and have given approval to the final version of the manuscript.

Notes

The authors declare no competing financial interest.

ACKNOWLEDGMENTS

L.Y.K. acknowledges the provision of a research scholarship from the NUS Graduate School for Integrative Sciences and Engineering (NGS). X.L. acknowledges the support of NSF CMMI Award #14-62946. The authors thank M. H. Hong for use of the laser interference lithography facilities.

REFERENCES

(1) Li, X.; Bohn, P. W. Metal-assisted Chemical Etching in HF/H_2O_2 Produces Porous Silicon. *Appl. Phys. Lett.* **2000**, *77*, 2572−2574.
(2) Huang, Z.; Geyer, N.; Werner, P.; de Boor, J.; Gösele, U. Metal-Assisted Chemical Etching of Silicon: A Review. *Adv. Mater.* **2011**, *23*, 285−308.
(3) Huang, J. Q.; Chiam, S. Y.; Tan, H. H.; Wang, S.; Chim, W. K. Fabrication of Silicon Nanowires with Precise Diameter Control Using Metal Nanodot Arrays as a Hard Mask Blocking Material in Chemical Etching. *Chem. Mater.* **2010**, *22*, 4111−4116.
(4) Kong, L.; Dasgupta, B.; Ren, Y.; Mohseni, P. K.; Hong, M.; Li, X.; Chim, W. K.; Chiam, S. Y. Evidences for Redox Reaction Driven Charge Transfer and Mass Transport in Metal-assisted Chemical Etching of Silicon. *Sci. Rep.* **2016**, *6*, 36582.
(5) Dejarld, M.; Shin, J. C.; Chern, W.; Chanda, D.; Balasundaram, K.; Rogers, J. A.; Li, X. Formation of High Aspect Ratio GaAs Nanostructures with Metal-assisted Chemical Etching. *Nano Lett.* **2011**, *11*, 5259−5263.
(6) Kim, S. H.; Mohseni, P. K.; Song, Y.; Ishihara, T.; Li, X. Inverse Metal-Assisted Chemical Etching Produces Smooth High Aspect Ratio InP Nanostructures. *Nano Lett.* **2015**, *15*, 641−648.
(7) Qu, Y.; Zhou, H.; Duan, X. Porous Silicon Nanowires. *Nanoscale* **2011**, *3*, 4060−4068.
(8) Mohseni, P. K.; Kim, S. H.; Zhao, X.; Balasundaram, K.; Kim, J. D.; Pan, L.; Rogers, J. A.; Coleman, J. J.; Li, X. GaAs Pillar Array-based Light Emitting Diodes Fabricated by Metal-assisted Chemical Etching. *J. Appl. Phys.* **2013**, *114*, 064909.
(9) Balasundaram, K.; Mohseni, P. K.; Shuai, Y. C.; Zhao, D.; Zhou, W.; Li, X. Photonic Crystal Membrane Reflectors by Magnetic Field-Guided Metal-Assisted Chemical Etching. *Appl. Phys. Lett.* **2013**, *103*, 214103.
(10) Liu, R.; Zhao, X.; Roberts, C.; Yu, L.; Mohseni, P. K.; Li, X.; Podolskiy, V.; Wasserman, D. Enhanced Optical Transmission Through MacEtch-fabricated Buried Metal Grating. *Adv. Mater.* **2016**, *28*, 1441−1448.
(11) Narasimhan, V. K.; Hymel, T. M.; Lai, R. A.; Cui, Y. Hybrid Metal-semiconductor Nanostructure for Ultrahigh Optical Absorption and Low Electrical Resistance at Optoelectronic Interface. *ACS Nano* **2015**, *9*, 10590−10597.
(12) Peng, K.; Wang, X.; Li, L.; Wu, X.; Lee, S. High-performance Silicon Nanohole Solar Cells. *J. Am. Chem. Soc.* **2010**, *132*, 6872−6873.
(13) Balasundaram, K.; Sadhu, J. S.; Shin, J. C.; Azeredo, B.; Chanda, D.; Malik, M.; Hsu, K.; Rogers, J. A.; Ferreira, P.; Sinha, S.; Li, X. Porosity Control in Metal-Assisted Chemical Etching of Degenerately Doped Silicon Nanowires. *Nanotechnology* **2012**, *23*, 305304.
(14) Chang, S.; Chuang, V. P.; Boles, S. T.; Ross, C. A.; Thompson, C. V. Densely Packed Arrays of Ultra-high-aspect-ratio Silicon Nanowires Fabricated using Block-copolymer Lithography and Metal-assisted etching. *Adv. Funct. Mater.* **2009**, *19*, 2495−2500.
(15) Hildreth, O. J.; Rykaczewski, K.; Fedorov, A. G.; Wong, C. P. A DLVO Model for Catalyst Motion in Metal-assisted Chemical Etching based upon Controlled Out-of-plane Rotational Etching and Force-displacement Measurement. *Nanoscale* **2013**, *5*, 961−970.
(16) Lai, C. Q.; Choi, W. K. Synthesis of Free-standing, Curved Si Nanowires through Mechanical Failure of a Catalyst during Metal Assisted Chemical Etching. *Phys. Chem. Chem. Phys.* **2014**, *16*, 13402−13408.
(17) Tsujino, K.; Matsumura, M. Morphology of Nanoholes Formed in Silicon by Wet Etching Solutions Containing HF and H_2O_2 at Different Concentrations using Silver Nanoparticles as Catalysts. *Electrochim. Acta* **2007**, *53*, 28−34.
(18) Hildreth, O. J.; Lin, W.; Wong, C. P. Effect of Catalyst Shape and Etchant Composition on Etching Direction in Metal-assisted Chemical Etching of Silicon to Fabricate 3D Nanostructures. *ACS Nano* **2009**, *3*, 4033−4042.
(19) Chang, C.; Sakdinawat, A. Ultra-high Aspect Ratio High-resolution Nanofabrication for Hard X-ray Diffractive Optics. *Nat. Commun.* **2014**, *5*, 1−7.
(20) Tiberio, R. C.; Rooks, M. J.; Chang, C.; Knollenberg, C. F.; Dobisz, E. A.; Sakdinawat, A. Vertical Directionality-controlled Metal-assisted Chemical Etching for Ultrahigh Aspect Ratio Nanoscale Structures. *J. Vac. Sci. Technol., B: Nanotechnol. Microelectron.: Mater., Process., Meas., Phenom.* **2014**, *32*, 06FI01.
(21) Güder, F.; Yang, Y.; Küçükbayrak, U. M.; Zacharias, M. Tracing the Migration History of Metal Catalysts in Metal-assisted Chemically Etched Silicon. *ACS Nano* **2013**, *7*, 1583−1590.
(22) Yoon, S.-S.; Khang, D.-Y. Direct Visualization of Etching Trajectories in Metal-Assisted Chemical Etching of Si by the Chemical Oxidation of Porous Sidewalls. *Langmuir* **2015**, *31*, 10549−10554.
(23) Rykaczewski, K.; Hildreth, O. J.; Wong, C. P.; Fedorov, A. G.; Scott, J. H. J. Guided Three-dimensional Catalyst Folding during Metal-assisted Chemical Etching of Silicon. *Nano Lett.* **2011**, *11*, 2369−2374.
(24) Warkiani, M. E.; Bhagat, A. A. S.; Khoo, B. L.; Han, J.; Lim, C. T.; Gong, H. Q.; Fane, A. G. Isoporous Micro/nanoengineered Membranes. *ACS Nano* **2013**, *7*, 1882−1904.
(25) Yang, H.; Zhao, D.; Chuwongin, S.; Seo, J.; Yang, W.; Shuai, Y.; Berggren, J.; Hammar, M.; Ma, Z.; Zhou, W. Transfer-printed Stacked Nanomembrane Lasers on Silicon. *Nat. Photonics* **2012**, *6*, 615−620.
(26) Wu, B.; Kumar, A.; Pamarthy, S. High Aspect Ratio Silicon Etch: A Review. *J. Appl. Phys.* **2010**, *108*, 051101.
(27) Peng, K.; Lu, A.; Zhang, R.; Lee, S. Motility of Metal Nanoparticles in Silicon and Induced Anisotropic Silicon Etching. *Adv. Funct. Mater.* **2008**, *18*, 3026−3035.

DOI: 10.1021/acsami.7b04565
ACS Appl. Mater. Interfaces 2017, 9, 20981−20990

(28) Lai, C. Q.; Cheng, H.; Choi, W. K.; Thompson, C. V. Mechanics of Catalyst Motion during Metal Assisted Chemical Etching of Silicon. *J. Phys. Chem. C* **2013**, *117*, 20802−20809.
(29) Lee, C.; Tsujino, K.; Kanda, Y.; Ikeda, S.; Matsumura, M. Pore Formation in Silicon by Wet Etching using Micrometer-sized Metal Particles as Catalysts. *J. Mater. Chem.* **2008**, *18*, 1015−1020.
(30) Han, H.; Huang, Z.; Lee, W. Metal-assisted Chemical Etching of Silicon and Nanotechnology Applications. *Nano Today* **2014**, *9*, 271−304.
(31) Hildreth, O. J.; Brown, D.; Wong, C. P. 3D Out-of-plane Rotational Etching with Pinned Catalysts in Metal-assisted Chemical Etching of Silicon. *Adv. Funct. Mater.* **2011**, *21*, 3119−3128.
(32) Brodoceanu, D.; Elnathan, R.; Prieto-Simón, B.; Delalat, B.; Guinan, T.; Kroner, E.; Voelcker, N. H.; Kraus, T. Dense Array of Uniform Submicron Pores in Silicon and Their Applications. *ACS Appl. Mater. Interfaces* **2015**, *7*, 1160−1169.
(33) Chartier, C.; Bastide, S.; Levy-Clément, C. L. Metal-assisted Chemical Etching of Silicon in HF-H_2O_2. *Electrochim. Acta* **2008**, *53*, 5509−5516.
(34) Peng, K.; Wang, X.; Wu, X.; Lee, S. Fabrication and Photovoltaic Property of Ordered Macroporous Silicon. *Appl. Phys. Lett.* **2009**, *95*, 143119.
(35) Kim, J. D.; Mohseni, P. K.; Balasundaram, K.; Ranganathan, S.; Pachamuthu, J.; Coleman, J. J.; Li, X. Scaling the Aspect Ratio of Nanoscale Closely Packed Silicon Vias by MacEtch: Kinetics of Carrier Generation and Mass Transport. *Adv. Funct. Mater.* **2017**, *27*, 1605614.
(36) Guo, L.; Ren, Y.; Kong, L. Y.; Chim, W. K.; Chiam, S. Y. Ordered Fragmentation of Oxide Thin Films at Submicron Scale. *Nat. Commun.* **2016**, *7*, 13148.
(37) Sundius, T. Computer Fitting of Voigt Profiles to Raman lines. *J. Raman Spectrosc.* **1973**, *1*, 471−488.
(38) Hochbaum, A. I.; Gargas, D.; Hwang, Y. J.; Yang, P. Single Crystalline Mesoporous Silicon Nanowires. *Nano Lett.* **2009**, *9*, 3550−3554.
(39) Qu, Y.; Liao, L.; Li, Y.; Zhang, H.; Huang, Y.; Duan, X. Electrically Conductive and Optically Active Porous Silicon Nanowires. *Nano Lett.* **2009**, *9*, 4539−4543.
(40) Chiappini, C.; Liu, X.; Fakhoury, J. R.; Ferrari, M. Biodegradable Porous Silicon Barcode Nanowires with Defined Geometry. *Adv. Funct. Mater.* **2010**, *20*, 2231−2239.
(41) Mikhael, B.; Elise, B.; Xavier, M.; Sebastian, S.; Johann, M.; Laetitia, P. New Silicon Architectures by Gold-assisted Chemical Etching. *ACS Appl. Mater. Interfaces* **2011**, *3*, 3866−3873.
(42) To, W. K.; Tsang, C. H.; Li, H. H.; Huang, Z. Fabrication of n-type Mesoporous Silicon Nanowires by One-step Etching. *Nano Lett.* **2011**, *11*, 5252−5258.
(43) Geyer, N.; Fuhrmann, B.; Huang, Z.; de Boor, J.; Leipner, H. S.; Werner, P. Model for the Mass Transport during Metal-assisted Chemical Etching with Contiguous Metal Films as Catalysts. *J. Phys. Chem. C* **2012**, *116*, 13446−13451.
(44) Geyer, N.; Wollschläger, N.; Fuhrmann, B.; Tonkikh, A.; Berger, A.; Werner, P.; Jungmann, M.; Krause-Rehberg, R.; Leipner, H. S. Influence of the Doping Level on the Porosity of Silicon Nanowires Prepared by Metal-assisted Chemical Etching. *Nanotechnology* **2015**, *26*, 245301.
(45) Zhong, X.; Qu, Y.; Lin, Y. C.; Liao, L.; Duan, X. Unveiling the Formation Pathway of Single Crystalline Porous Silicon Nanowires. *ACS Appl. Mater. Interfaces* **2011**, *3*, 261−270.
(46) McSweeney, W.; Glynn, C.; Geaney, H.; Collins, G.; Holmes, J. D.; O'Dwyer, C. Mesoporosity in Doped Silicon Nanowires from Metal Assisted Chemical Etching Monitored by Phonon Scattering. *Semicond. Sci. Technol.* **2016**, *31*, 014003.
(47) Ratchford, D.; Yeom, J.; Long, J. P.; Pehrsson, P. E. Influence of Inhomogeneous Porosity on Silicon Nanowire Raman Enhancement and Leaky Mode Modulated Photoluminescence. *Nanoscale* **2015**, *7*, 4124−4133.
(48) Kiraly, B.; Yang, S.l; Huang, T. J. Multifunctional Porous Silicon Nanopillar Arrays: Antireflection, Superhydrophobicity, Photoluminescence, and Surface-enhanced Raman Ccattering. *Nanotechnology* **2013**, *24*, 245704.
(49) Cerdeira, F.; Fjeldly, T. A.; Cardona, M. Effect of Free Carriers on Zone-center Vibrational Modes in Heavily Doped p-type Si. II. Optical Modes. *Phys. Rev. B* **1973**, *8*, 4734.
(50) Burke, B. G.; Chan, J.; Williams, K. A.; Wu, Z.; Puretzky, A. A.; Geohegan, D. B. Raman Study of Fano Interference in p-type Doped Silicon. *J. Raman Spectrosc.* **2010**, *41*, 1759−1764.
(51) Ghosh, R.; Pal, A.; Giri, P. K. Quantitative Analysis of the Phonon Confinement Effect in Arbitrarily Shaped Si Nanocrystals Decorated on Si Nanowires and its Correlation with the Photoluminescence Spectrum. *J. Raman Spectrosc.* **2015**, *46*, 624−631.
(52) Adu, K. W.; Gutiérrez, H. R.; Kim, U. J.; Eklund, P. C. Inhomogeneous Laser Heating and Photon Confinement in Silicon Nanowires: A Micro-Raman Scattering Study. *Phys. Rev. B: Condens. Matter Mater. Phys.* **2006**, *73*, 155333.
(53) Rodichkina, S. P.; Osminkina, L. A.; Isaiev, M.; Pavlikov, A. V.; Zoteev, A. V.; Georgobiani, V. A.; Gonchar, K. A.; Vasiliev, A. N.; Timoshenko, V. Y. Raman Diagnostics of Photoinduced Heating of Silicon Nanowires Prepared by Metal-assisted Chemical Etching. *Appl. Phys. B: Lasers Opt.* **2015**, *121*, 337−344.
(54) Israelachvili, J. N. *Intermolecular and Surface Forces*, 3rd ed.; Academic Press: London, 1992; pp 254−256.
(55) Verlet, L. Computer "Experiments" on Classical Fluids. I. Thermodynamical Propertyies of Lennard-Hones Molecules. *Phys. Rev.* **1967**, *159*, 98−103.
(56) Geyer, N.; Fuhrmann, B.; Leipner, H. S.; Werner, P. Ag-Mediated Charge Transport during Metal-Assisted Chemical Etching of Silicon Nanowires. *ACS Appl. Mater. Interfaces* **2013**, *5*, 4302−4308.
(57) Létant, S. E.; Hart, B. R.; van Buuren, A. W.; Terminello, L. J. Functionalized Silicon Membranes for Selective Bio-organism Capture. *Nat. Mater.* **2003**, *2*, 391−395.

DOI: 10.1021/acsami.7b04565
ACS Appl. Mater. Interfaces 2017, 9, 20981−20990